Double diffusive layer formation near a cooled liquid–solid boundary

E. JURJEN KRANENBORG and HENK A. DIJKSTRA†

Institute for Marine and Atmospheric Research Utrecht, Utrecht University, The Netherlands

Abstract—As an idealization of convection near an ice boundary, flows in both salt-stratified and non-stratified liquids generated by a cooled slab of solid material are considered through direct numerical simulation. When the liquid far from the slab is homogeneous, significant convection occurs below the ice and apart from a small boundary layer, hardly no flow appears next to the ice. On the contrary, when the background liquid is stratified through a constant salt gradient, a layered flow appears next to the ice if the thickness of the slab is large enough. The latter flows are of double diffusive origin and have a significant effect on the transport of heat and salt near the ice. © 1998 Elsevier Science Ltd. All rights reserved.

1. INTRODUCTION

Step structures in vertical profiles of salinity and temperature, for example as observed in the ocean, are characteristic signatures of double diffusive processes, i.e. convection in a stably stratified liquid induced by the different molecular diffusivities of two components [1]. A typical situation of layered flow occurs in a salt stratified liquid over which a horizontal temperature difference is applied. These type of flows have been studied in the laboratory for idealized situations, for example in rectangular containers [2–4]. Theoretical work has focussed on the critical conditions for the double diffusive instabilities to occur [5] and their subsequent evolution to well-developed layers [6, 7].

In case the initial temperature T_i is constant and the initial salinity S_i a linear function of height, layers with a characteristic scale

$$\eta = \frac{\alpha \Delta T}{\phi_0} \tag{1a}$$

appear when a Rayleigh number Ra_η, based on η, is large enough. In equation (1a), ϕ_0 is the background density gradient $[-\beta(\partial S_i/\partial z)]$ and ΔT the horizontal temperature difference. The parameters α and β are the coefficients in the linear equation of state relating changes in the temperature and salinity to those in the density, respectively. The initial scale of the layers may be substantially smaller, but subsequent merging of layers leads eventually to a layer thickness with scale η. An analysis of this layer merging process is given in ref. [8].

When, in addition to a stable salinity gradient, a destabilizing temperature gradient is initially present, and if the stability ratio

$$R_\rho = \frac{\beta \dfrac{\partial S_i}{\partial z}}{\alpha \dfrac{\partial T_i}{\partial z}} \tag{1b}$$

is small enough, layers may propagate even when the lateral cooling has been turned off. This so-called self-propagation has been experimentally observed by ref. [9] and its physics was analysed through direct numerical simulation in ref. [10].

A typical situation where one expects these layered flows in the ocean is near ice boundaries, for example slabs of sea-ice or icebergs, which provide the lateral cooling of the stably stratified liquid. Motivated by the fact that these flows significantly influence the melting of the ice, Huppert and Turner [11, 12] performed the first laboratory experiments on double diffusive flows near ice bodies. It was shown that, when a block of ice is put into a liquid which is stably stratified through a constant salt gradient, the layer thickness also scales with η. In this case, the lateral temperature difference ΔT must be taken as the difference between the temperature at the ice boundary (with freezing point based on the far field salinity) and that of the liquid far from the ice. The layered flows were shown to be of double diffusive origin. The melting of an ice wall in a cavity filled with water of uniform salinity [13] is completely different. In this case and at oceanic ambient salinities, the transport of meltwater relatively far from the wall is downward. However, next to the ice wall the liquid may become buoyant, because the dilution effect due to the melting of the ice may be dominant over the cooling effect. In any case, no layered flow appears.

† Author to whom correspondence should be addressed. Institute for Marine and Atmospheric Research Utrecht, Utrecht University, Princetonplein 5, 3584 CC, Utrecht, The Netherlands. Tel. 31-30-2533276. Fax: 31-30-254163. E-mail: h.a.dijkstra@fys.ruu.nl.

NOMENCLATURE

A	aspect ratio		β	solutal expansion coefficient [—]
D	thickness of the ice slab [m]		ΔS	vertical salinity difference [—]
g	gravitational acceleration [m s^{-2}]		ΔT	horizontal temperature difference [K]
h	layer thickness [m]		η	internal vertical lengthscale [m]
H	length of half of the ice slab [m]		Θ	dimensionless temperature in the ice slab
Le	Lewis number		Θ^*	dimensional temperature in the ice slab [K]
p	dimensionless pressure			
Pr	Prandtl number		κ_S	saline diffusivity [m^2 s^{-1}]
R	buoyancy ratio		κ_T	thermal diffusivity of water [m^2 s^{-1}]
R_ρ	vertical stability ratio		κ_Θ	thermal diffusivity of ice [m^2 s^{-1}]
Ra_η	thermal Rayleigh number based on η		λ	ratio of thermal diffusivities of ice and water
Ra_T	thermal Rayleigh number based on H			
S	dimensionless salinity		ν	kinematic viscosity [m^2 s^{-1}]
S^*	salinity [—]		ρ	dimensionless density
t	dimensionless time		ϕ_0	initial density gradient [m^{-1}]
t^*	time [s]		Φ_T	dimensionless heat flux
T	dimensionless temperature		Φ_S	dimensionless salt flux.
T^*	temperature [K]			
$\mathbf{u}$	dimensionless velocity vector		Subscripts	
u	dimensionless horizontal velocity		cr	critical
w	dimensionless vertical velocity		i	initial
x	dimensionless horizontal coordinate		0	reference.
z	dimensionless vertical coordinate.			
			Superscripts	
Greek symbols			h	horizontal
α	thermal expansion coefficient [K^{-1}]		v	vertical.

The double diffusive flows considered experimentally in ref. [14], using lower ambient temperatures and smaller salinity gradients than those in [12], showed a similar layer formation (with the same layer scale). In polar areas, it is common that the background salinity $S_i(z)$ and temperature $T_i(z)$ decrease upwards in the upper layers of the ocean. Based on the above mentioned laboratory experiments, one would expect layer formation near ice boundaries. These layered structures have indeed been observed, for example by ref. [15] near a 150 m ice face in the South Cape Fiord in the Arctic.

One might question how thick such an ice body should be for layered flows to appear. For example, can these flows develop near relatively thin sheets of sea-ice? Another issue of interest is how the transport of heat and salt is altered by these double diffusive flows, in comparison with direct buoyancy driven flows near the ice. Both questions are addressed in this paper, where we study flows near (an idealization of) an ice slab through a direct numerical simulation in a two-dimensional set-up. It is found that the thickness of the slab has to be larger than the internal length scale η for layered flows to appear. The heat and mass transport of the buoyancy driven flows is strongly modified when layers are present, for example

the vertical salt and heat transport next to the ice is strongly reduced.

2. MODEL FORMULATION AND NUMERICAL IMPLEMENTATION

In the present numerical study, an ice plate is represented by a cooled slab of solid material. This simplification makes sense since both a cooled cylinder and an ice slab result in the same type of flows [12], while in the former case there are no effects of ice melting on the flow. The slab (length $2H$, thickness D, thermal diffusivity κ_Θ and temperature Θ) is cooled from above and partially covers a water column in a rectangular container (Fig. 1(a)) in which a stable initial salinity gradient is present (thermal diffusivity κ_T, diffusivity of salt κ_S, kinematic viscosity ν, temperature T^* and salinity S^*). Due to symmetry, only half of the container and half of the slab are presented in Fig. 1a; the right boundary in Fig. 1(a) is an axis of symmetry.

A linear equation of state with respect to a constant reference temperature T_0 and salinity S_0 is assumed, i.e. $\rho = \rho_0(1 - \alpha(T^* - T_0) + \beta(S^* - S_0))$. The governing, equations are non-dimensionalized using scales H, H^2/κ_T and κ_T/H for length, time and velocity,
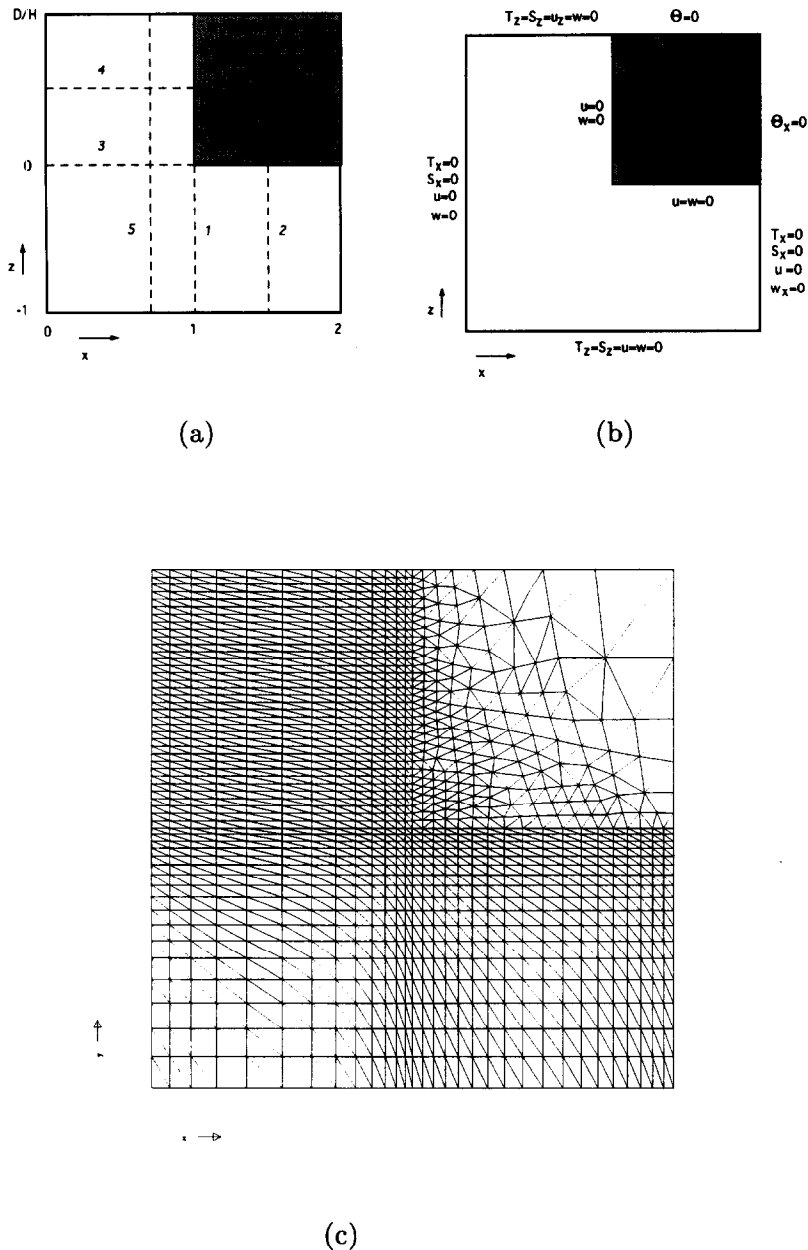
(a)

(b)

(c)

Fig. 1. (a) Geometrical set-up of the problem; (b) Summary of the boundary conditions prescribed; (c) Typical finite element mesh as used for the thick slab simulation.

respectively. The temperature and salinity are non-dimensionalized by $T = (T^* - T_0)/\Delta T$, $\Theta = (\Theta^* - T_0)/\Delta T$ and $S = (S^* - S_0)/\Delta S$, where ΔS and ΔT are typical vertical salinity and horizontal temperature differences, respectively. With this scaling, the container wall is located at $x = 0$, the vertical solid–liquid boundary at $x = 1$, and the symmetry axis at $x = 2$. The bottom of the container is located at $z = -1$, the horizontal solid–liquid boundary at $z = 0$, and both the upper slab boundary and the top of the liquid at $z = D/H$. These boundaries are indicated in Fig. 1(a)

and along the indicated sections, profiles and transport properties are presented below.

In primitive variables, the dimensionless governing equations become

$$Pr^{-1}\left(\frac{\partial \mathbf{u}}{\partial t} + (\mathbf{u} \cdot \nabla)\mathbf{u}\right) = -\nabla p + \nabla^2 \mathbf{u} + \hat{\mathbf{z}} Ra_\mathrm{T}(T - RS)$$

(2a)

$$\nabla \cdot \mathbf{u} = 0 \qquad (2b)$$

$$\frac{\partial T}{\partial t} + (\mathbf{u} \cdot \nabla)T = \nabla^2 T \qquad (2c)$$

$$\frac{\partial S}{\partial t} + (\mathbf{u} \cdot \nabla)S = Le^{-1} \nabla^2 S \qquad (2d)$$

where $\hat{z}$ is the unit vector in vertical direction. The heat transfer in the solid is modeled by the heat equation

$$\frac{\partial \Theta}{\partial t} = \lambda \nabla^2 \Theta. \qquad (3)$$

At the fixed solid–liquid boundary continuity of temperature and heat flux is expressed as

$$T = \Theta, \quad \nabla T \cdot \mathbf{n} = \lambda \nabla \Theta \cdot \mathbf{n} \qquad (4)$$

where $\mathbf{n}$ is the normal on the boundary.

Along the container walls (left and lower boundary) no-slip conditions and no-flux conditions for both heat and salt are prescribed. At the symmetry axis, free-slip conditions and no-flux conditions for heat and salinity apply. The top of the slab is cooled through a constant temperature Θ_0^*. At the solid–liquid interface no-slip conditions, no-flux salinity conditions and conditions (4) are prescribed. Finally, at the upper boundary of the liquid free-slip conditions and no-flux conditions for temperature and salinity are prescribed. The boundary conditions of the problem are summarized in Fig. 1(b).

The dimensionless parameters which appear in equations (2)–(4) are the Rayleigh number Ra_T, the buoyancy ratio R, the Prandtl number Pr, the Lewis number Le and the diffusivity ratio λ, defined as

$$Ra_T = \frac{g\alpha\Delta T H^3}{\nu\kappa_T}, \quad R = \frac{\beta\Delta S}{\alpha\Delta T},$$

$$Pr = \frac{\nu}{\kappa_T}, \quad Le = \frac{\kappa_T}{\kappa_S}, \quad \lambda = \frac{\kappa_\Theta}{\kappa_T}. \qquad (5a)$$

Using the layer thickness scale η, a Rayleigh number Ra_η, based in η, can be expressed into model parameters as

$$R = H/\eta; \quad Ra_\eta = Ra_T/R^3. \qquad (5b)$$

A standard Galerkin finite element method [16], using quadratic elements for the velocity, temperature and salinity, and linear elements for the pressure, was applied to equations (2)–(4). This finite element discretization is second order accurate in space. A penalty formulation is used to eliminate the pressure unknowns. The nonlinear terms are linearized using the standard Newton–Raphson method and the resulting sets of linear equations are solved using a direct (profile) solver.

The spatial resolution chosen depends on the thickness of the slab and the value of Ra_η. The lowest resolution is used with a relatively thin slab and uses 31 elements in the horizontal and 21 elements in the vertical (which amounts to 9577 unknowns), while the highest resolution (for a thick slab) corresponds to 64 elements in the horizontal and 75 elements in the vertical (49 832 unknowns). An example of a typical mesh in the latter case is shown in Fig. 1(c) showing an

Table 1. Standard dimensionless and dimensional parameters in this study

$H = 0.2$ (m)	$Ra_\eta = 5 \cdot 10^4$
$L = 0.2$ (m)	$R = 2.5$
$\kappa_S = 1 \cdot 10^{-9}$ (m^2 s^{-1})	$Pr = 6.7$
$\kappa_T = 1 \cdot 10^{-7}$ (m^2 s^{-1})	$Le = 100$
$\kappa_\Theta = 1 \cdot 10^{-6}$ (m^2 s^{-1})	$\lambda = 10$
$\nu = 7 \cdot 10^{-7}$ (m^2 s^{-1})	

Table 2. Summary of the different cases considered

Situation	Plate thickness D	$S(x, z; t = 0)$
A (reference)	$D = H$	$S = 1 - z$
B	$D = 0.1H$	$S = 1 - z$
C	$D = H$	$S = 1$
D	$D = 0.1H$	$S = 1$

increased resolution near the solid–liquid boundary. Time integration is performed using the implicit Crank–Nicolson method except for the first two iterations where the Euler method is used. Both the resolution and the time step (dimensionless values range between 10^{-5} and 10^{-4}) were chosen such that halving grid space and time step gave similar results during the initial stages of evolution of the flow for the typical case 'A' below.

3. FLOW DEVELOPMENT

In the results below, the standard values of the parameters are shown in Table 1. This reference model can be regarded as an extension of one of the cavity models with aspect ratio $A = 1$ as investigated in ref. [8]. To analyse specific double diffusive signatures the four different cases as shown in Table 2 are considered. Differences appear through the thickness of the slab and the presence or absence of a stable initial stratification.

3.1. Stratified background

Case 'A' represents a stratified liquid which is cooled by a relatively thick plate of thickness $D = H$. From the substitution of $H = D$ in $R = H/\eta$ it follows from $D/\eta = R = 2.5$, i.e. the thickness of the plate is larger than the internal layer scale. The initial conditions consists of a homogeneous temperature and a linear salinity distribution, i.e.

$$t = 0 : T(x, z) = 1; \quad S(x, z) = 1 - z; \quad \Theta(x, z) = 1. \qquad (6)$$

The time-dependent evolution up to $t = 5.5 \cdot 10^{-2}$ (in dimensional units $t^* = 2.2 \cdot 10^4$ [s]) is shown in Fig. 2 through contour plots of the temperature and salinity and a vector plot of the velocity field at four different times during this evolution. Initially, a
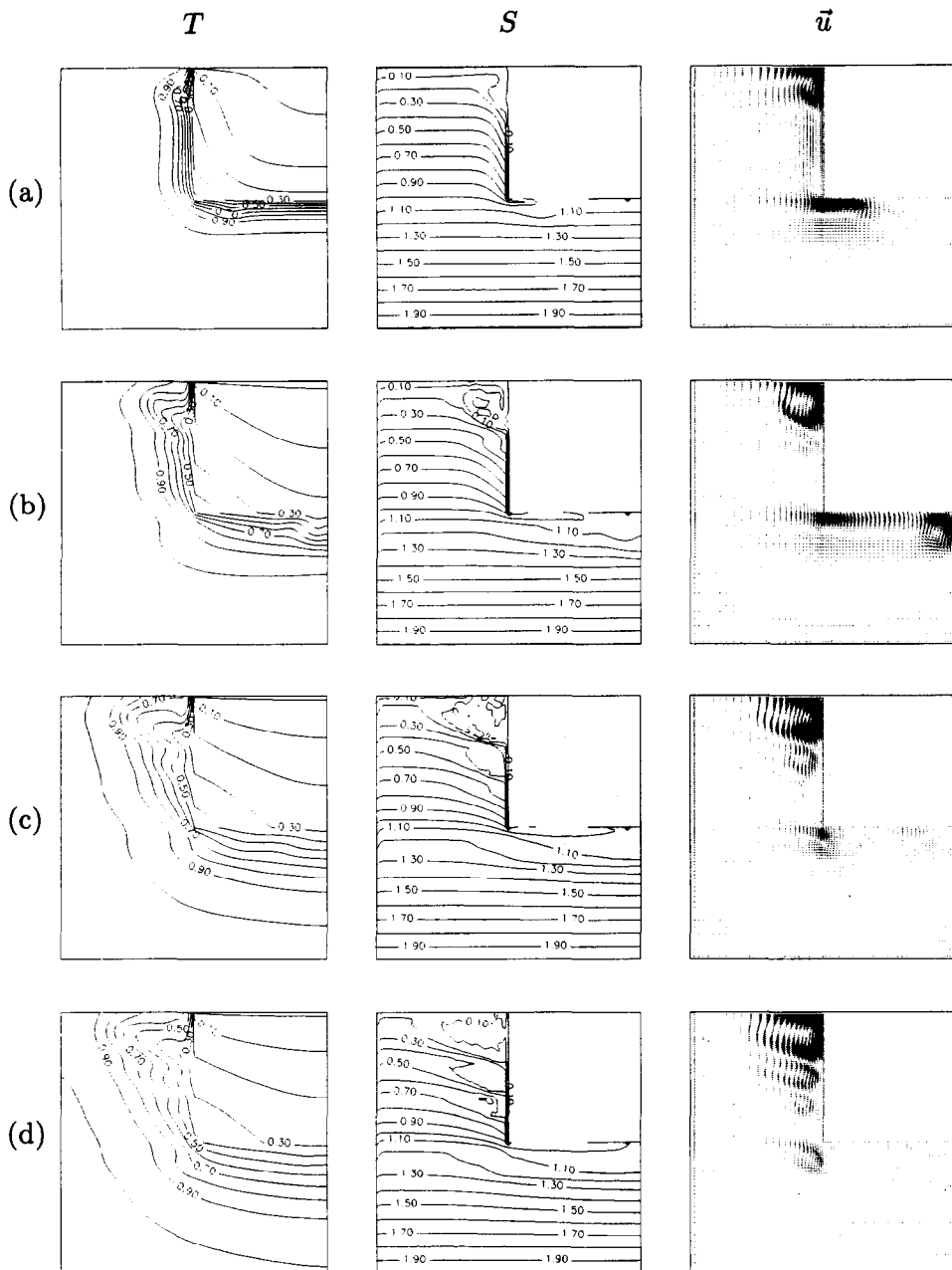
Fig. 2. Development in time of the temperature, salinity and velocity distribution, case 'A', $Ra_\eta = 5 \cdot 10^4$; (a) $t = 5 \cdot 10^{-3}$ $(2.0 \cdot 10^3$ s); (b) $t = 1.5 \cdot 10^{-2}$ $(6.0 \cdot 10^3$ s); (c) $t = 3.5 \cdot 10^{-2}$ $(1.4 \cdot 10^4$ s); (d) $t = 5.5 \cdot 10^{-2}$ $(2.2 \cdot 10^4$ s).

diffusive thermal boundary layer forms near the boundaries of the slab (Fig. 2(a)). A strong downward flow is induced next to the wall transporting fresh water downwards which considerably reduces the salinity near the ice. This boundary layer flow becomes unstable through double diffusive instabilities and layers start to form (Fig. 2(b) and (c)). Convection is stronger at the top because the horizontal temperature difference is largest.

Near the corner of the slab ($x = 1, z = 0$), the isotherms of the boundary layer are necessarily curved

and hence a horizontal density gradient is set-up. Because the density is larger just below the horizontal wall of the plate, the convection cell near the corner has a clockwise rotation (Fig. 2(a)). Warmer liquid is transported under the ice, maintaining the horizontal gradient and the cell propagates to the right (Fig. 2(b)). Since this flow is caused by the asymmetry in the forcing, due to the geometry, we will refer to it as an geometrically induced flow.

Although the latter (forced) convection is present below the ice slab, layer formation occurs along the
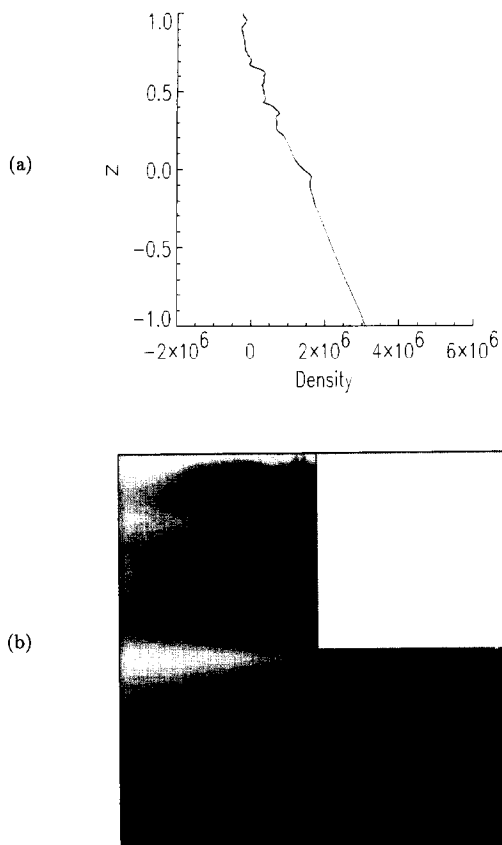
Fig. 3. (a) Vertical density distribution along section 5; (b) Grayscale plot of the anomalous salinity distribution (difference of actual and initial salinity) for case 'A', $Ra_\eta = 5 \cdot 10^4$. Light (dark) regions indicate a higher (lower) salinity than the initial salinity.

complete vertical boundary of the slab and is much more intense. At the time when the flow has become quasi-stationary (Fig. 2(d)), the distribution of the density field (Fig. 3(a)) along section 5 (Fig. 1(a)) shows the characteristic step structures associated with the layers. Near $z = 0$, the density gradient changes substantially and the liquid slightly above $z = 0$ is much more stable than that immediately below $z = 0$. This jump is expected to strongly influence the vertical transport since the liquid below $z = 0$ is not easily mixed with the liquid above, in other words a 'shielding effect' occurs.

The layered structures, as well as the exchange of salt due to the geometrically induced flow can be more clearly observed in the grayscale plot of the anomalous salinity distribution (difference with respect to the initial salinity) in Fig. 3(b). The vertical lengthscale h of the layers can be estimated from Fig. 2(d) and 3(b) and it is found that the ratio h/D is about 0.24. Since D/η equals the buoyancy ratio $R = 2.5$ (based on the initial salinity profile), the ratio h/η is about 0.60. There exists a close agreement between the layer development next to the plate and the initial layer devel-

opment in the square cavity simulation in ref. [8] for $R = 2.5$. First, from Fig. 4 in ref. [8] we calculate that the ratio h/D for the middle layer at $t = 0.05$ is about 0.3. With $D/\eta = 2.5$, the value of h/η becomes 0.8 which is slightly larger than the value obtained above for slab cooling. The latter difference is attributed to the fact that in ref. [8] the overall temperature difference is slightly larger because the temperature along the wall is homogeneous, whereas for the slab, it decreases downward along the wall. The timescale of the development of the layers in both cases is quite similar. In the slab model, the second convection cell has advanced roughly over a distance $\Delta x = 0.5$ at $t = 0.055$. In Fig. 4 of ref. [8], a similar scale for Δx is found at $t = 0.05$.

In case 'B', the slab thickness is significantly smaller than the internal layer scale ($D/\eta = 0.1 R = 0.25$). The patterns of the temperature and salinity (Fig. 4(a)) do not show any signatures of layer formation. On the contrary, there is strong mixing both next to and below the slab, the latter component again geometrically induced as can be seen from the velocity distribution. The latter flow strongly modifies the flow next to the slab resulting in the absence of step structures in the density profile (Fig. 4(b)). The results indicate that the slab should be sufficiently thick (larger than the internal lengthscale η) for the layers to develop. If the slab is thinner, a fluid element initially near the top of the layer that is descending along the slab must pass the corner of the slab before it can turn back inside the liquid. At that point the fluid element is necessarily influenced by the geometrically induced flow.

The value of Ra_η applied in the previous simulations is rather small compared to that in experiments performed by [12]. Therefore, we increased the Rayleigh number while keeping R constant, which can be regarded as increasing the value of H while keeping other scales constant. In particular, when H is increased by a factor three, $Ra_\eta = 1.35 \cdot 10^6$ results. For this value of Ra_η the computations are very expensive and only the initial stages of flow development were computed (up to $t = 5 \cdot 10^{-3}$ or $t^* = 1.8 \cdot 10^4$ [s]). Since time scales with H^2, the same dimensional time t^* is reached at $t = 4.5 \cdot 10^{-2}$ for the standard case $Ra_\eta = 5 \cdot 10^4$. The results for $Ra_\eta = 1.35 \cdot 10^6$ are shown in Fig. 5(a) ('A') and Fig. 5(b) ('B') reveal a strong convective activity both next to as well as below the slab. Along the vertical slab wall for case 'A', a layered pattern develops similar to the simulation with $Ra_\eta = 5 \cdot 10^4$ but with a slightly smaller thickness. This smaller scale appears because the simulation time is too small for subsequent layer merging to occur. In case 'B' no layered flow pattern develops for similar reasons as explained above. Again, most of the convective activity occurs below the slab. For both cases 'A' and 'B', significant convection is seen below the ice (Fig. 5) contrary to that in Fig. 2(a) and 4(a). This is likely due to diffusive instabilities through vertical gradients [17], which have destabilized the
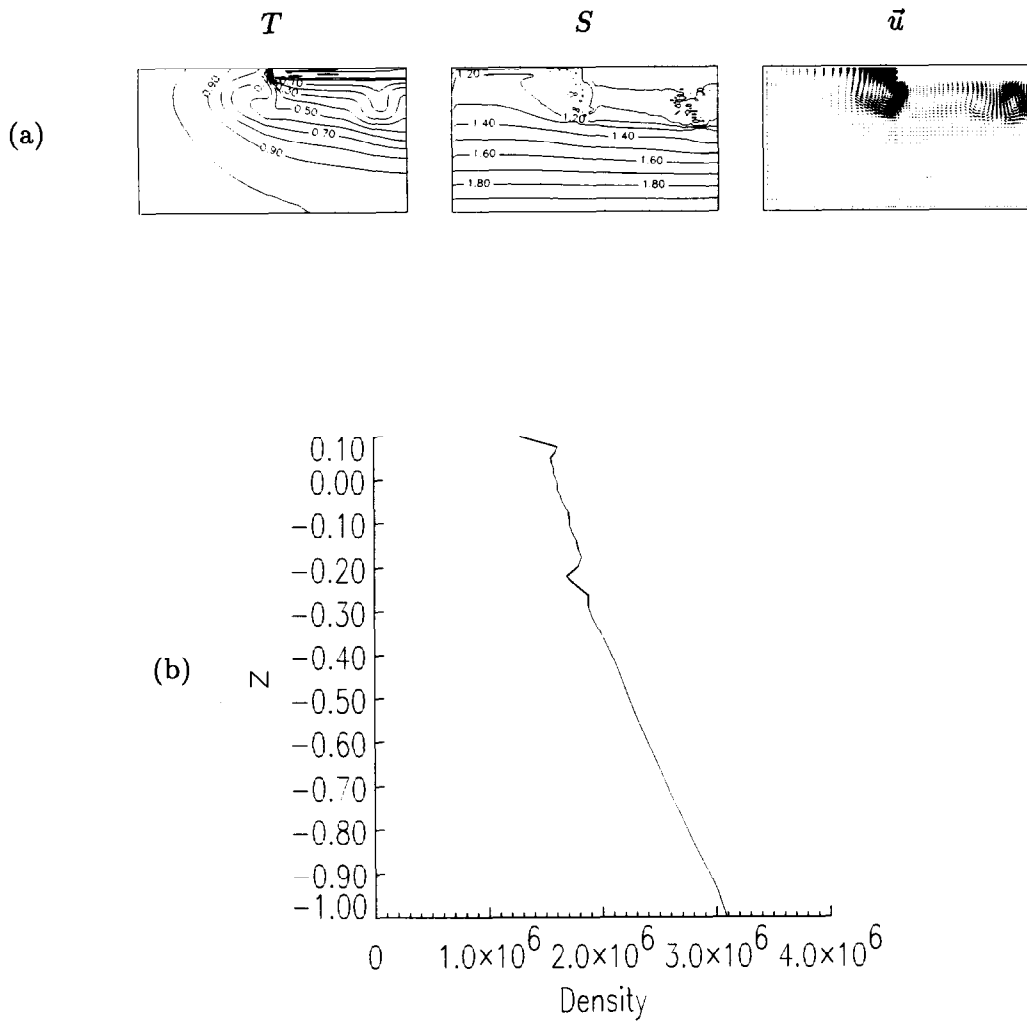
T S $\vec{u}$

(a)

(b) N

0.10
0.00
−0.10
−0.20
−0.30
−0.40
−0.50
−0.60
−0.70
−0.80
−0.90
−1.00

0   1.0×10^{6} 2.0×10^{6} 3.0×10^{6} 4.0×10^{6}

Density

Fig. 4. (a) Temperature, salinity and velocity distributions at $t = 5.5\cdot10^{-2}$ $(2.2\cdot10^{4}$ s) for the stratified case 'B', $Ra_{\eta} = 5\cdot10^{4}$; (b) vertical density distribution along section 5.

T S $\vec{u}$

(a)

(b)

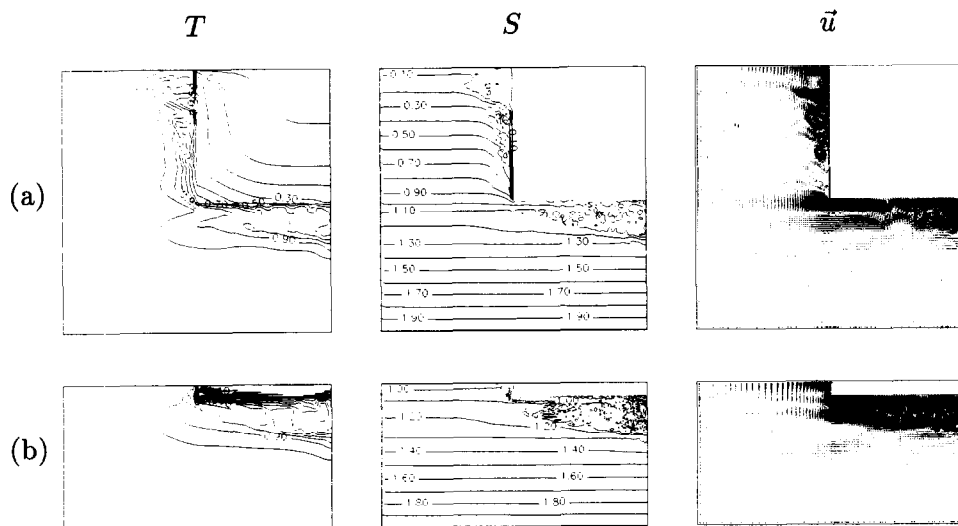

Fig. 5. Temperature, salinity and velocity distributions at $t = 5\cdot10^{-3}$ $(1.8\cdot10^{4}$ s) for the stratified cases, $Ra_{\eta} = 1.35\cdot10^{6}$; (a) case 'A'; (b) case 'B'.

thermal boundary layer below the slab. Its signatures are the formation of a well-mixed layer which is growing downwards through entrainment [18].

3.2. *Non-stratified background*

Cases 'C' and 'D' are equivalent to cases 'A' and 'B' but with the absence of the initial salinity gradient. Hence, the initial state consists of both homogeneous temperature and salinity distributions, i.e.

$$t = 0 : T(x, z) = 1 ; \quad S(x, z) = 1 ; \quad \Theta(x, z) = 1. \quad (7)$$

Note that if the salinity is homogeneous initially, it remains constant during the evolution since a constant solute concentration is compatible with the boundary conditions. Hence, only the flow due to the cooling of the liquid by thermally induced buoyancy is considered. In this way, the signatures of double-diffusive convection and, in particular, its influence on the heat and mass transport can be determined.

For the thick slab (Fig. 6(a)), a narrow thermal boundary layer forms next to the slab, of which the thickness increases downwards. This is a classical boundary layer for which the thickness scales with $Ra^{-1/4}$, where the Rayleigh number is based on the
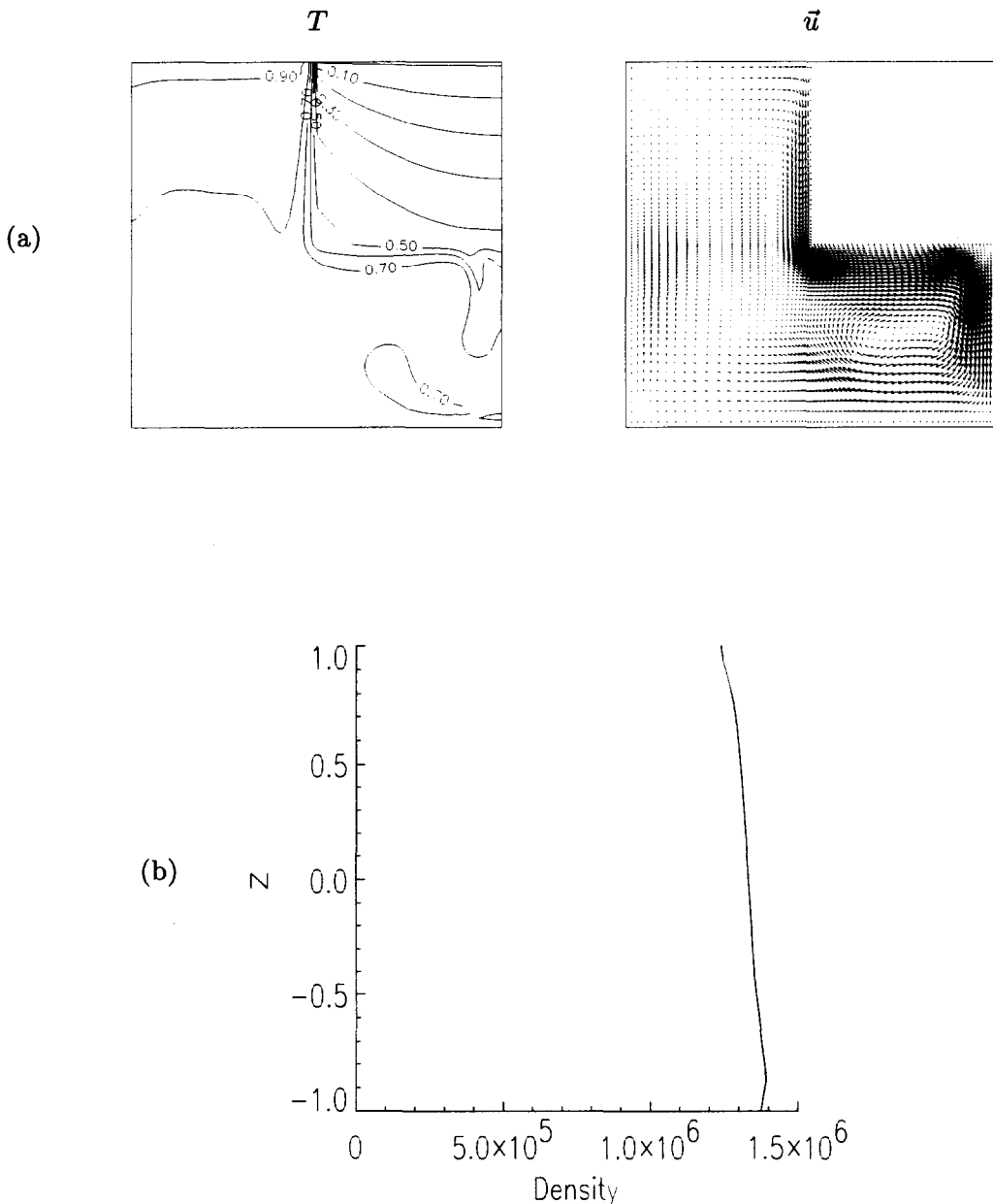

Fig. 6. (a) Temperature and velocity distributions for $Ra_\eta = 5 \cdot 10^4$ at $t = 5.5 \cdot 10^{-2}$ for the non-stratified case 'C' ; (b) vertical density distribution along section 5.
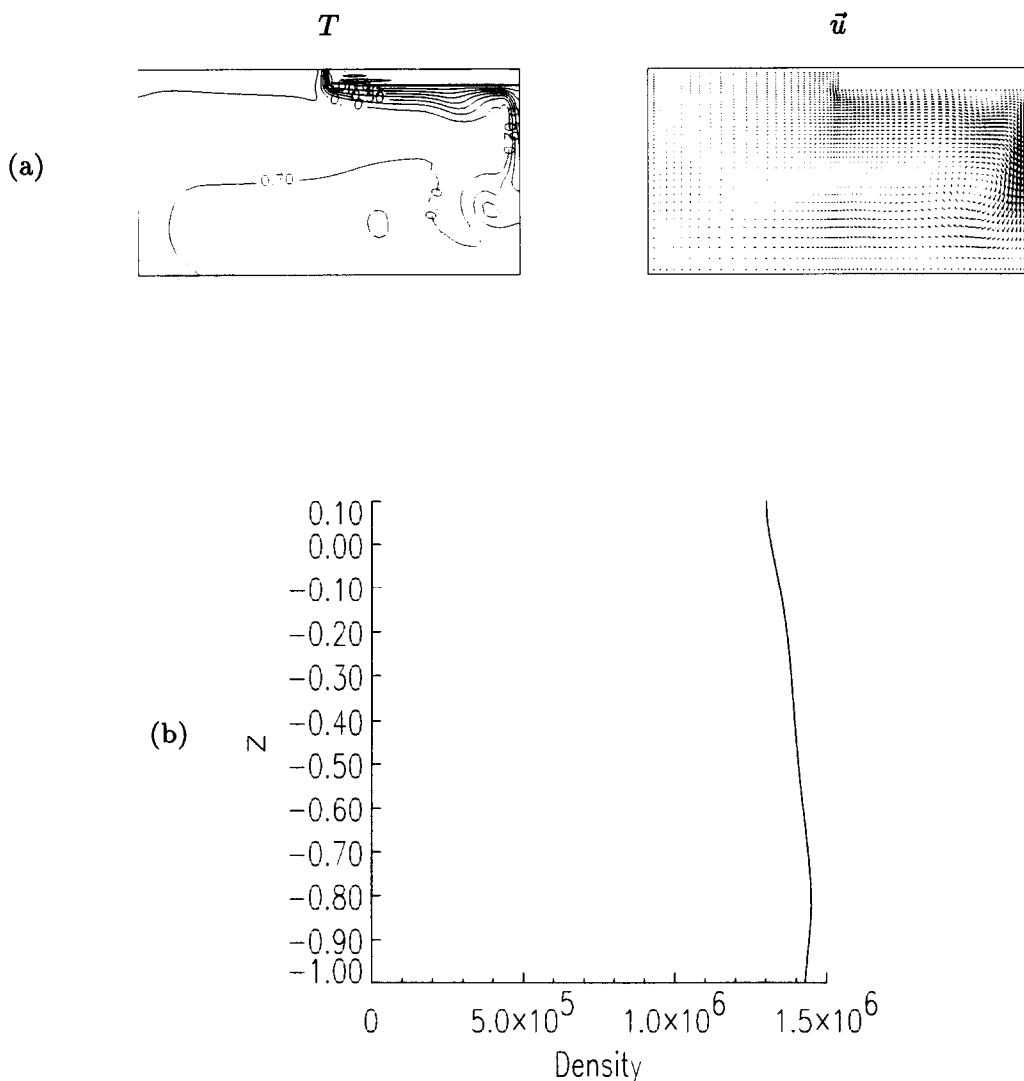
T $\vec{u}$

(a)

(b)

Fig. 7. (a) Temperature and velocity distributions for $Ra_\eta = 5 \cdot 10^4$ at $t = 5.5 \cdot 10^{-2}$ for the non-stratified case 'D'; (b) Vertical density distribution along section 5.

distance along the slab boundary. The flow below the slab is again geometrically induced by horizontal density gradients and occupies the whole region below the slab. No step structures in the density at section 5 are present (Fig. 6(b)) demonstrating that these are characteristic features of double diffusive processes. For the thin slab, the boundary layer next to the ice has a near constant thickness and the convection below the ice is much weaker because the temperature gradient in the ice is much smaller (Fig. 7(a)). Apart from that, the flow is very similar to that of the thick slab in that no appreciable flow appears next to the ice resulting in nearly the same density profile as that in Fig. 6(b) at section 5 (Fig. 7(b)).

For $Ra_\eta = 1.35 \cdot 10^6$, snapshots of the flows in the cases 'C' and 'D' are shown in Fig. 8(a) and (b), respectively. The boundary layer thickness next to the ice is smaller, as expected, and convection is much

more intense below the ice. However, still no appreciable flow develops far from the slab next to the ice. This picture is in qualitative agreement with the experimental results of ref. [19] which also show a thermally induced vigorous flow just below an ice surface. With a lengthscale equal to half of the length of the slab and a temperature difference of order $O(1)$ between the ice slab and the bulk of the liquid, the Rayleigh number Ra_η is about $3.2 \cdot 10^6$, near the value used in our simulation.

3.3. Heat and mass transfer

An analysis of the heat and mass transport of the flows computed above is considered through the values of the integrated transport across the sections depicted in Fig. 1(a). The horizontal heat and salt fluxes across sections 1 and 2 are defined as
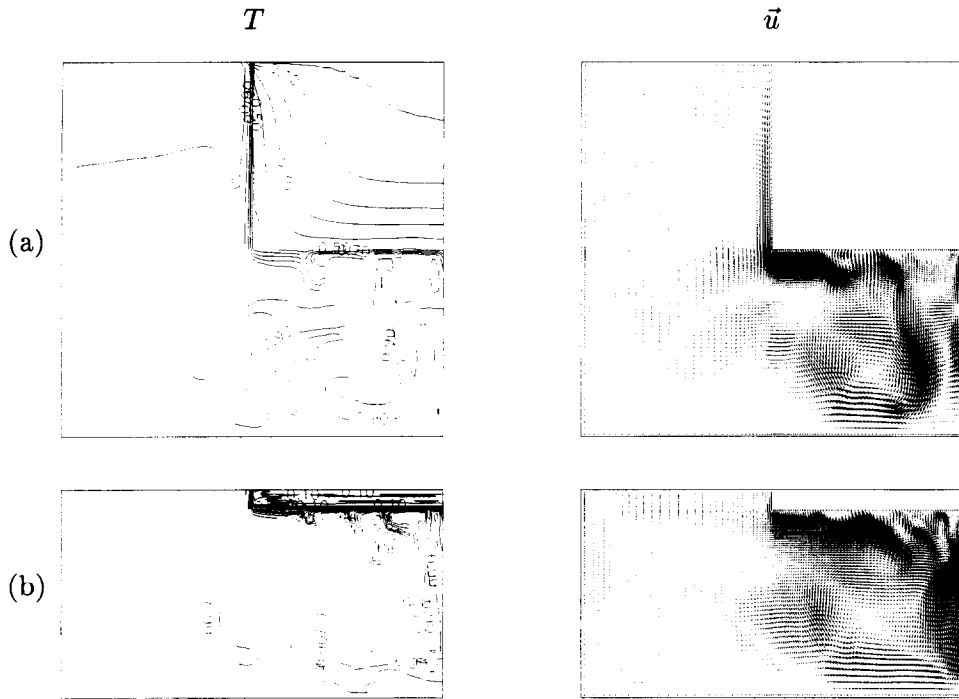
$$T \qquad\qquad\qquad \vec{u}$$

(a)

(b)

Fig. 8. Temperature distributions at $t = 5 \cdot 10^{-3}$ for the nonstratified cases, $Ra_n = 1.35 \cdot 10^6$; (a) case 'C'; (b) case 'D'.

$$\Phi_T^h = \int_{z=-1}^{z=0} [uT - \partial T/\partial x]_{x=x_i} \, \mathrm{d}z \, ;$$

$$\Phi_S^h = \int_{z=-1}^{z=0} [uS - Le^{-1} \, \partial S/\partial x]_{x=x_i} \, \mathrm{d}z \qquad (8\mathrm{a})$$

whereas the vertical fluxes across sections 3 and 4 are computed through

$$\Phi_T^v = \int_{x=0}^{x=1} [wT - \partial T/\partial z]_{z=z_j} \, \mathrm{d}x \, ;$$

$$\Phi_S^v = \int_{x=0}^{x=1} [wS - Le^{-1} \, \partial S/\partial z]_{z=z_j} \, \mathrm{d}x. \qquad (8\mathrm{b})$$

In Fig. 9, the evolution of the salt fluxes along the sections 1 and 3 is shown for case 'A'. These fluxes are not expected to change significantly beyond the simulation time, unless subsequent layer merging occurs leading to a different flow pattern. Nevertheless, these flows are (at best) quasi-stationary and the calculations on the heat and mass transport represent only snapshots. However, the results should be sufficient to determine the qualitative differences of the transport between the flow considered. The heat and salt fluxes across the sections 1–4 for the cases 'A–D'. ($Ra_n = 5 \cdot 10^4$) are presented in Table 3 and 4, respectively. A positive value indicates transport of the particular quantity in the positive x- or z-direction.

The reduction of vertical heat transport due to layer formation can be immediately seen by comparing the
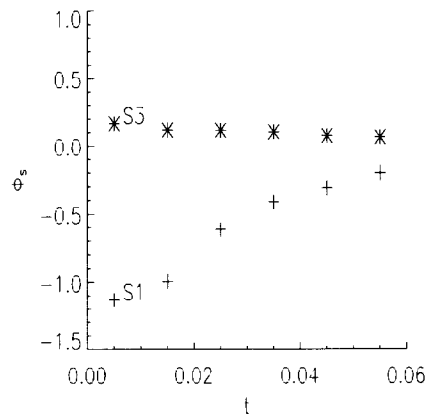
Fig. 9. The temporal development of salt fluxes Φ_S along sections 1 (S1) and 3 (S3) for case 'A'.

Table 3. Integrated heat fluxes along sections indicated in Fig. 1a, $t = 4.5 \cdot 10^{-2}$, $Ra_n = 5 \cdot 10^4$

Case	Section 1	Section 2	Section 3	Section 4
A	0.143	0.085	0.493	0.593
B	0.672	−0.513	1.50	0.952
C	−0.530	1.02	2.84	3.07
D	2.48	0.055	1.25	0.764

Table 4. Integrated salt fluxes along sections indicated in Fig. 1a, $t = 4.5 \cdot 10^{-2}$, $Ra_\eta = 5 \cdot 10^4$

Case	Section 1	Section 2	Section 3	Section 4
A	−0.310	−0.123	0.076	−0.023
B	−0.387	−0.424	0.437	0.349

heat transport through the sections 3 and 4 for the cases 'A' and 'B' (Table 3). Both values are significantly smaller for case 'A', indicating that the 'shielding effect' has a pronounced effect on the vertical transport of heat. The same follows for the vertical salt transport which is mainly upwards at both sections in case 'B', but upwards at section 3 in case 'A' and downwards at section 4 (Table 4). The latter result indicates that the layered flow also causes a strong reduction in the vertical transport of salt, and that salt transport is mainly lateral.

Below the slab, the lateral heat transport is also much smaller in case 'A' than in case 'B' along section 1 (Table 3). This is a consequence of the strong geometrically induced flow in case 'B' (Fig. 4(a)), where warm water is mixed under the ice; this effect is much smaller in case 'A' (Fig. 2(d)). The same flow can explain the different heat transport along section 2. The salt transport is to the left-along both sections 1 and 2 (Table 4), due to the return flow far below the ice. This net transport is partly responsible for the strong stratification near $z = 0$, inducing the buoyancy jump associated with the 'shielding effect' in case 'A', as discussed below.

The vertical transport of heat in the non-stratified case takes place mainly within the boundary layer near the slab. Since the flow is downward and the ice cools the liquid, the effective heat transport is upwards resulting in the positive values in Table 3 for the cases 'C' and 'D'. The boundary layer flow is much stronger for the thick slab (compare Fig. 6(a) and 7(a)) resulting in much larger values for the heat transport along sections 3 and 4 in case 'C'. Since the flow below the ice is likely to be very intermittent, not much value can be put on the actual numbers of the horizontal heat transport along the sections 1 and 2; these are at most indicative.

4. DISCUSSION

In this paper, we considered buoyancy driven flows in a liquid near a cooled solid boundary. The liquid has either a constant background salinity or is stratified through a constant salinity gradient. In both cases, the average salinity is large enough such that a linear equation of state is applicable. Through the idealization of the ice as a non-deformable boundary dilution effects due to the melting of the ice were not considered. Also the effect of the freezing point depression due to salinity was neglected. Both features

may be important in 'real' convection near ice boundaries, but are out of the scope of this study. Furthermore it was shown in refs. [7, 9] that, under oceanographical conditions, meltwater has a negligible effect on the structure and thickness of the layers. Concentrating on the induced convection patterns, we consider the non-deformable slab idealization to be appropriate.

It was shown that the two types of flow are completely different. In the non-stratified case, the flow in a thin boundary layer near the ice is responsible for the vertical transport of heat and salt next to the ice. Hardly any flow develops outside this boundary layer. Vigorous convection develops below the ice, forced by the temperature gradients in the ice. The thickness of the slab plays a minor role and although the intensity of the flow does depend on Ra_η, the overall character does not.

On the contrary, for the flows developing in the stratified environment, the lateral cooling of the liquid results, through double diffusive processes, in the formation of horizontal layers with a characteristic lengthscale η. For the particular case 'A' investigated, the result $h/\eta = 0.6$ compares quite well with the scales as reported by ref. [12] and presented in their Tables 1–3. For example, considering experiments no. 2 and no. 3 in their Table 1, experiments no. 1, no. 6 and no. 8 in their Table 2, and experiment no. 14 in their Table 3, we see that for values of Ra_η close to $5 \cdot 10^4$ the corresponding values of h/η are in the range [0.56, 0.98]. Moreover, our particular value is close to the value of $h/\eta = 0.65$ they propose based on all experiments. The double-diffusive flow next to the slab appears to be little influenced by the flows in other regions due to the buoyancy jump generated at the lower slab edge. This jump arises through both the appearance of layers and the geometrically induced flow. Since the salinity is low near the ice, relatively fresh-water is transported to the left by the convection just above $z = 0$ (Fig. 2(d) and 3(b)). By the geometrically induced flow, salt is transported upwards just below $z = 0$ (Fig. 2(d)) resulting in the density jump near $z = 0$. The resulting 'shielding effect' was shown to have a substantial impact on the vertical transport of heat and salt near the ice.

For layers to appear, it is necessary that the thickness of the slab is larger than the length scale η. A layered flow will not develop due to lateral gradients if the thickness is smaller than η because the flow is disturbed by the geometrically induced flow below the ice. In oceanographic measurements of step structures [15], the density gradient in the ocean is three orders of magnitude smaller and Ra_η is a factor 10^8 larger. This leads to scales η of the order 0.1–0.2 [m]. These layers can therefore indeed be attributed to sideways cooling due to an ice slab and both sea-ice and icebergs will be able to induce them. However, it may not be easy to distinguish the origin of the layers in terms of the destabilizing background temperature gradient. For example, all measurements used in ref. [20] to

compute overall mixing coefficients due to double diffusive processes assume that these layered flows are caused by a vertical destabilizing heat flux (through diffusive instabilities [17]). However, the layers may just as well be caused by sideways cooling, for example through icebergs, which are likely to be present at some of the locations. The origin of the layers is therefore an important issue, since different layer scales may result and thereby differing mixing coefficients.

REFERENCES

1. Schmitt, R. W., Double diffusion in oceanography. *Ann. Rev. Fluid Mech.*, 1994, **26**, 255–285.
2. Chen, C. F., Briggs, D. G. and Wirtz, R. A., Stability of thermal convection in a salinity gradient due to lateral heating. *International Journal of Heat and Mass Transfer*, 1971, **14**, 57–65.
3. Tanny, J. and Tsinober, A. B., The dynamics and structure of double-diffusive layers in sidewall-heating experiments. *Journal of Fluid Mechanics*, 1988, **196**, 135–156.
4. Jeevaraj, C. and Imberger, J., Experimental study of double-diffusive instability in sidewall heating. *Journal of Fluid Mechanics*, 1991, **222**, 565–586.
5. Thangam, S., Zebib, A. and Chen, C. F., Transition from shear to sideways diffusive instability in a vertical slot. *Journal of Fluid Mechanics*, 1981, **112**, 151–160.
6. Kerr, O. S., Heating a salinity gradient from a vertical sidewall: nonlinear theory. *Journal of Fluid Mechanics*, 1990, **217**, 529–546.
7. Dijkstra, H. A. and Kranenborg, E. J., A bifurcation study of double diffusive flows in a laterally heated stably stratified liquid. *International Journal of Heat and Mass Transfer*, 1996, **39**, 2699 2710.
8. Kranenborg, E. J. and Dijkstra, H. A., The evolution of double-diffusive intrusions into a stably stratified liquid: A study of the layer merging process. *International Journal of Heat and Mass Transfer*, 1998, in press.
9. Schladow, S. G., Thomas, E. and Koseff, J. R., The dynamics of intrusions into a thermohaline stratification, *Journal of Fluid Mechanics*, 1992, **236**, 127–165.
10. Dijkstra, H. A. and Kranenborg, E. J., The evolution of double-diffusive intrusions into a stably stratified liquid: The physics of self-propagation. *International Journal of Heat and Mass Transfer*, 1998, in press.
11. Huppert, H. E. and Turner, J. S., On melting icebergs. *Nature*, 1978, **271**, 46–48.
12. Huppert, H. E. and Turner, J. S., Ice blocks melting into a salinity gradient. *Journal of Fluid Mechanics*, 1980, **100**, 367–384.
13. Josberger, E. G. and Martin, S., A laboratory and theoretical study of the boundary layer adjacent to a vertical melting ice wall in salt water. *Journal of Fluid Mechanics*, 1981, **111**, 439–473.
14. Huppert, H. E. and Josberger, E. G., The melting of ice in cold stratified water. *Journal of Physical Oceanography*, 1980, **10**, 953–960.
15. Horne, E. P. W., Ice-induced vertical circulation in an Arctic fiord. *J. Geophys. Research*, 1985, **90**, C1, 1078–1086.
16. Segal, A., SEPRAN user manual. SEPRA Analysis, The Netherlands, 1994.
17. Baines, P. G. and Gill, A. E., On thermohaline convection with linear gradients. *Journal of Fluid Mechanics*, 1969, **37**, 289–306.
18. Molemaker, M. J. and Dijkstra, H. A., Layer formation in a stably stratified liquid cooled from above. *Double Diffusive Convection*, ed. A. Brandt and H. J. S. Fernando, Geophysical Monograph, 1995, **94**, 97–104.
19. Gebhart, B., Sammakia, B. and Audunson, T., Melting characteristics of horizontal ice surfaces in cold saline water. *J. Geophys. Research*, 1983, **88**, C5, 2935–2942.
20. Kelley, D. E., Effective diffusivities within ocean thermohaline staircases. *J. Geophys. Res.*, 1984, **89**, 10 484–10 499.